Bismuth-based heterometallic clusters capped by calixarene for visible-light photothermal conversion

Tianxia Chen, Yuhan, Zou, Dongao, Mao, Yanfeng Bi*

School of Petrochemical Engineering, Liaoning Petrochemical University, Fushun 113001, P. R. China.

*Corresponding author: biyanfeng@lnpu.edu.cn (Y. F. Bi)

1. Photothermal experiment

A 30 mg sample was placed on quartz flakes paving 1 cm^2 rounds for solid photothermal conversion, and a certain amount of the sample was dispersed in 0.5 mL $CHCl_3$ in a centrifuge tube to configure the required concentrations for the liquid photothermal experiment and then irradiated using a 520 nm wavelength lamp. The sample temperature was recorded on FL-IR infrared thermography. The distance between the sample and lamp was fixed at 10 cm. A quartz flake (343 mg) was placed over the sample to investigate its solid photothermal conversion efficiency. All the experiment was carried out at 20 °C.

2. Determine the solvent molecules in Bi_2Co_4

The residual electron density of **Bi_2Co_4** was treated as a diffuse contribution using SQUEEZE. There are 939 $Å^3$ voids with 168 estimated electrons occupied by solvents (DMF and H_2O). After combining the analysis of the size, electron number, and void volume, it was estimated that each unit cell contained 3 DMF (40 e^-) molecules and 2 H_2O (10 e^-) molecules. The Formula for **Bi_2Co_4** is $[BiCo_2(HTC4A)_2(CH_3COO)]_2(DMF)_3(H_2O)_2$.

```
# SQUEEZE RESULTS (APPEND TO CIF)
# Note: Data are Listed for all Voids in the P1 Unit Cell
# i.e. Centre of Gravity, Solvent Accessible Volume,
# Recovered number of Electrons in the Void and
# Details about the Squeezed Material
loop_
 _platon_squeeze_void_nr
 _platon_squeeze_void_average_x
 _platon_squeeze_void_average_y
 _platon_squeeze_void_average_z
```

```
 _platon_squeeze_void_volume
 _platon_squeeze_void_count_electrons
 _platon_squeeze_void_content
  1 -0.500  0.500  0.000       827       154 ' ' ※
  2  0.310  0.730  0.505        47         6 ' ' *
  3  0.389  0.065  0.427         9         1 ' ' *
  4  0.690  0.270  0.495        47         6 ' ' *
  5  0.611  0.935  0.573         9         1 ' ' *
_platon_squeeze_details
```

※ Possibly occupied by 3 DMF molecules

* Possibly occupied by 2 H_2O molecules

3. Determine the solvent molecules in Bi_2Ni_4

The residual electron density of **Bi_2Ni_4** was treated as diffuse contributions using the program SQUEEZE. There are 936 $Å^3$ voids with 124 estimated electrons occupied by solvents (DMF and H_2O). After combining the analysis of the size, electron number, and void volume, it was estimated that each unit cell contained 3 DMF (40 e^-) molecules and 2 H_2O (10 e^-) molecules. The Formula for **Bi_2Ni_4** is $[BiNi_2(HTC4A)_2(CH_3COO)]_2(DMF)_3(H_2O)_2$.

```
# SQUEEZE RESULTS (APPEND TO CIF)
# Note: Data are Listed for all Voids in the P1 Unit Cell
# i.e. Centre of Gravity, Solvent Accessible Volume,
# Recovered number of Electrons in the Void and
# Details about the Squeezed Material
loop_
 _platon_squeeze_void_nr
 _platon_squeeze_void_average_x
 _platon_squeeze_void_average_y
 _platon_squeeze_void_average_z
 _platon_squeeze_void_volume
 _platon_squeeze_void_count_electrons
 _platon_squeeze_void_content
  1 -0.500  0.500  0.000       836       109 ' ' ※
  2  0.300  0.725  0.513        50         7 ' ' *
  3  0.700  0.275  0.487        50         8 ' ' *
_platon_squeeze_details
```

※ Possibly occupied by 3 DMF molecules

* Possibly occupied by 2 H_2O molecules

Figures

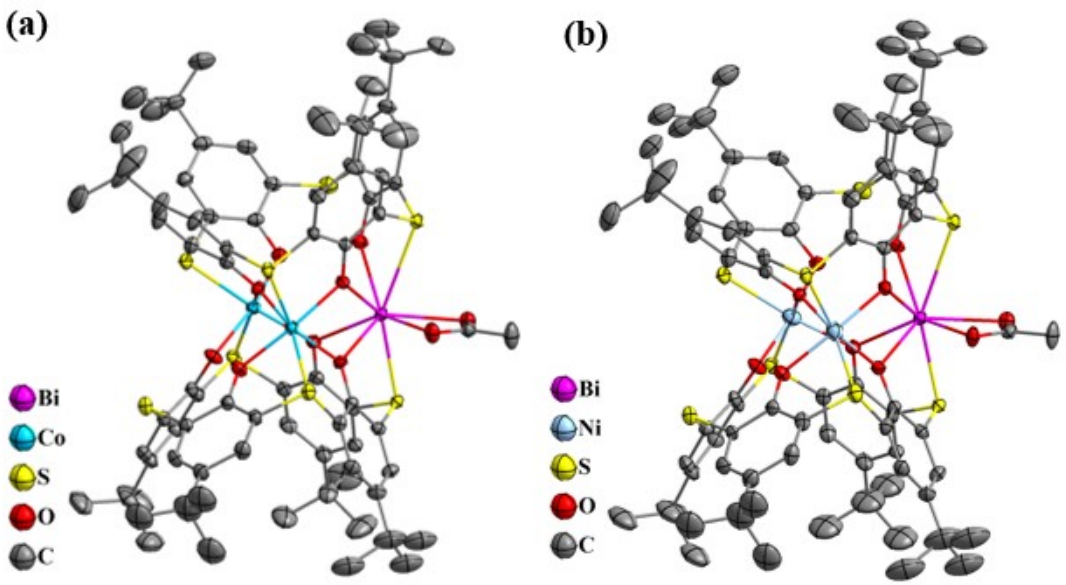

Fig. S1 Asymmetric Unit Ellipsoid of (a) **Bi_2Co_4** and (b) **Bi_2Ni_4**. (30 % probability used for Ellipsoid) (all H atoms and solvent molecules were omitted for clarity)

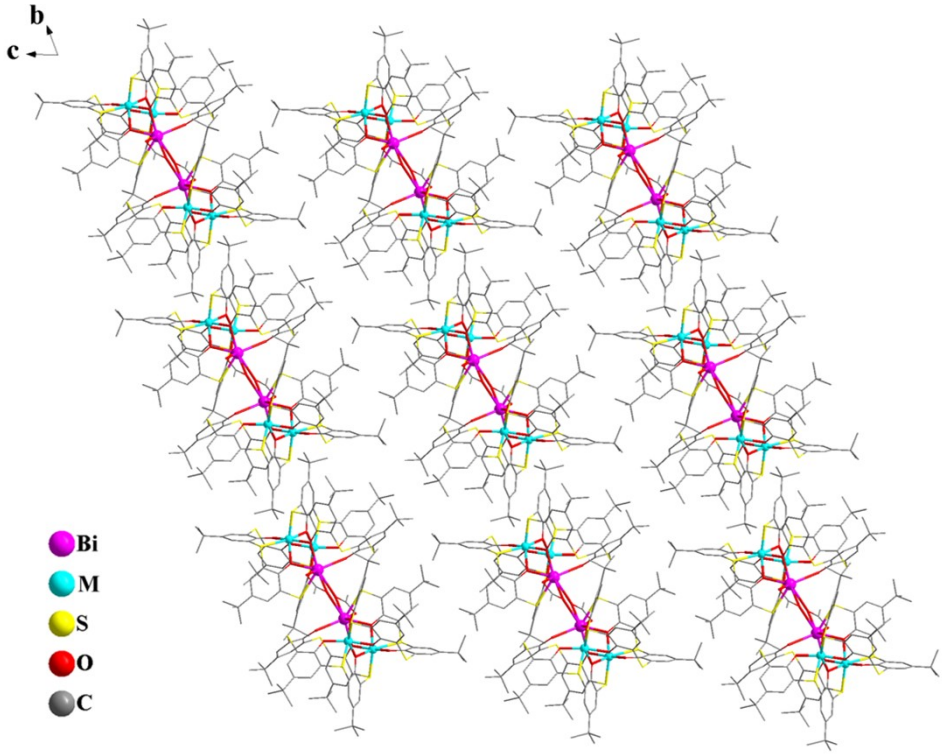

Fig. S2 Packing diagram along the a-axis of Bi_2M_4 (all H atoms and solvent molecules

were omitted for clarity)

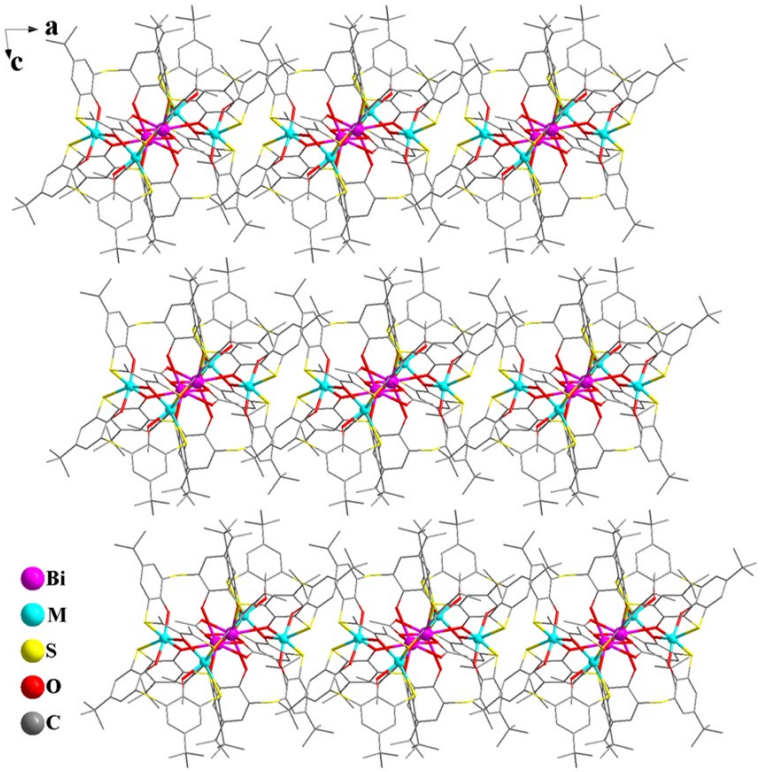

Fig. S3 Packing diagram along the b-axis of Bi_2M_4 (all H atoms and solvent molecules were omitted for clarity)

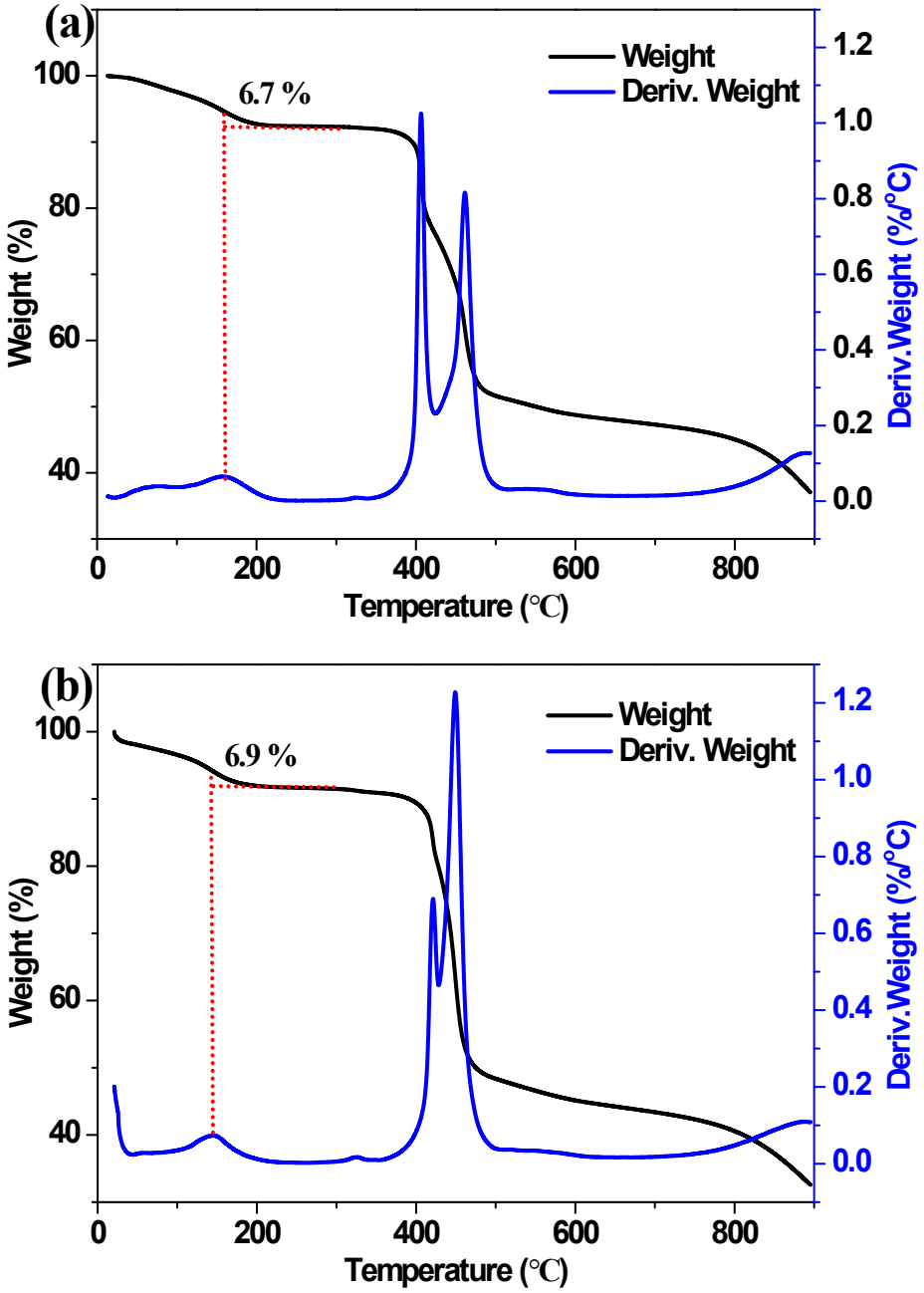

Fig. S4 TGA curve of (a) Bi_2Co_4 and (b) Bi_2Ni_4.

The thermogravimetric experiment was conducted from room temperature to 900 °C at 10 °C/min under the N_2 (100 mL/min). The experiments show that both Bi_2Co_4 and Bi_2Ni_4 had similar weight loss curves and maintained the skeleton below 400 °C. The curve indicates that the weight loss of Bi_2Co_4 is ca.6.7 % and Bi_2Ni_4 is ca.6.9 % below 160 °C, which are correlated to the value of three DMF and two H_2O from the SQUEEZE program (ca. 6.5%).

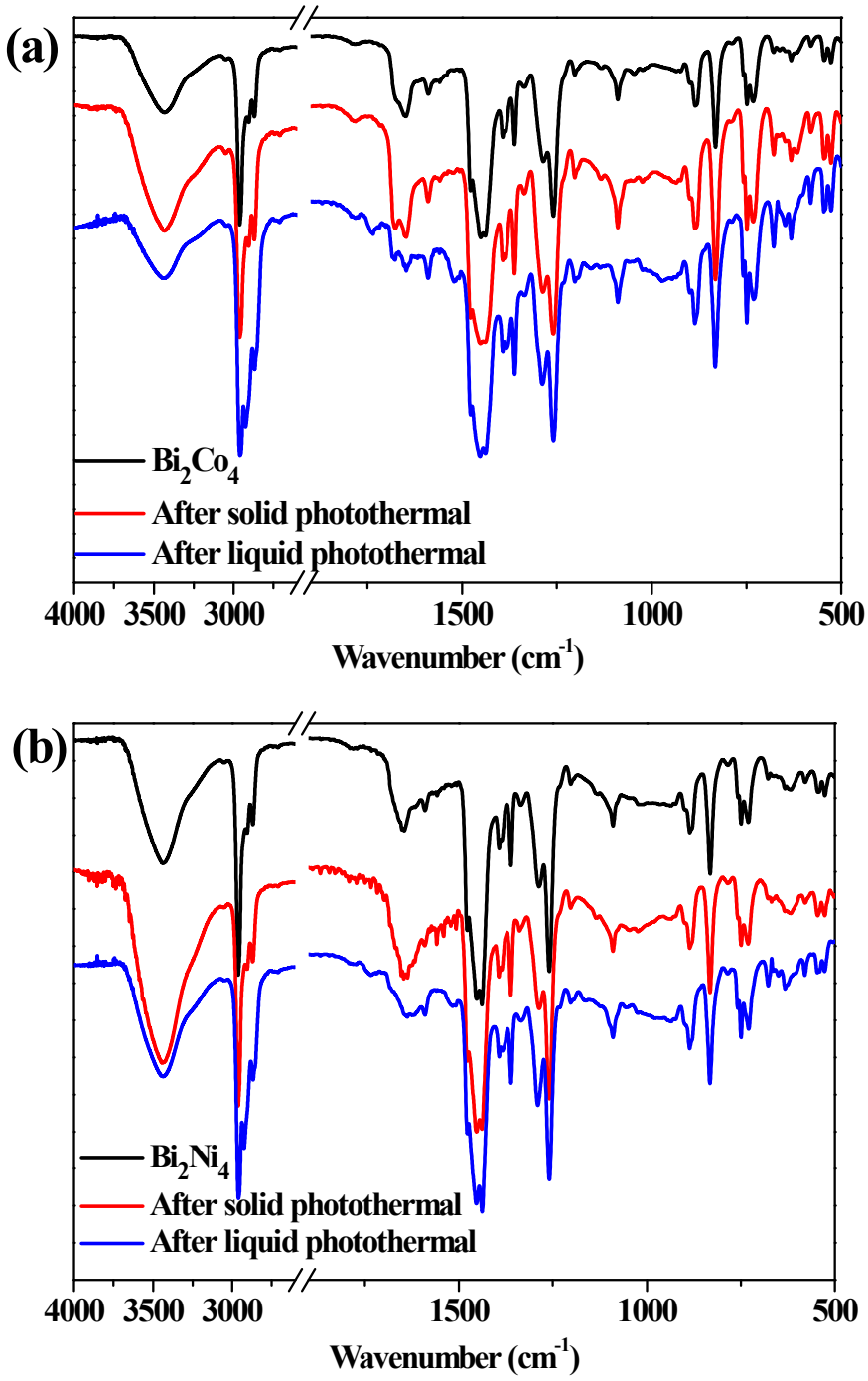

Fig. S5 FT-IR spectra of (a) **Bi_2Co_4** and (b) **Bi_2Ni_4**.

Peaks at 2960 cm^{-1}, 1450 cm^{-1}, and 1261 cm^{-1} ascribe to C-H, -CH_3, and C-O groups of calixarene, respectively. Peaks at 1581 cm^{-1}, 1387 cm^{-1}, and 1357 cm^{-1} were ascribed to -COO^-.[S1-S3] The FI-IR spectra after light irradiation of Bi_2M_4 are consistent with the initial curve which proved the stability of Bi_2M_4 during the photothermal experiment.

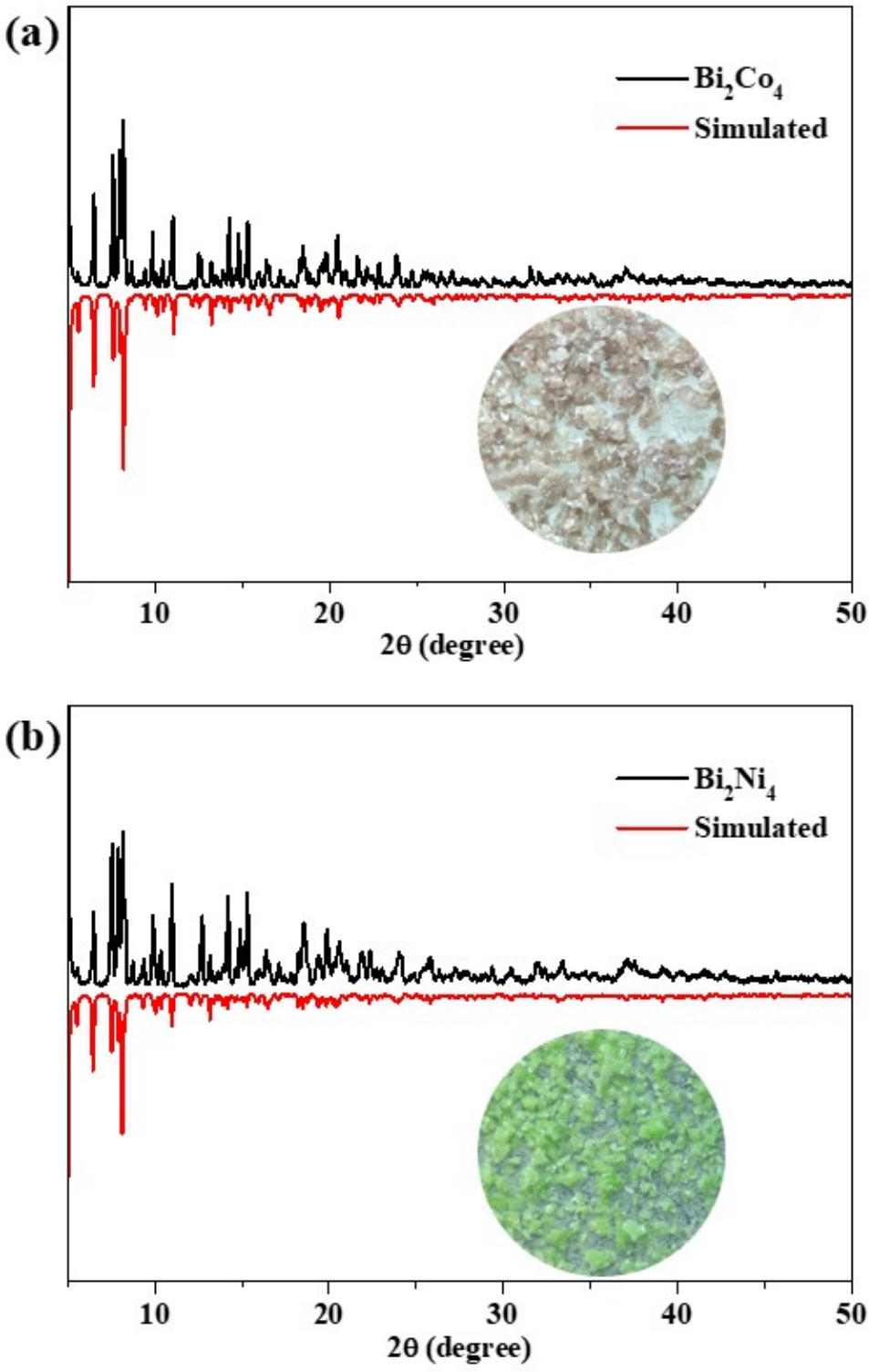

Fig. S6 PXRD of (a) **Bi_2Co_4** and (b) **Bi_2Ni_4**.

The powder X-ray diffraction (PXRD) patterns of Bi_2M_4 are well-matched with the simulated patterns derived from the single crystal.

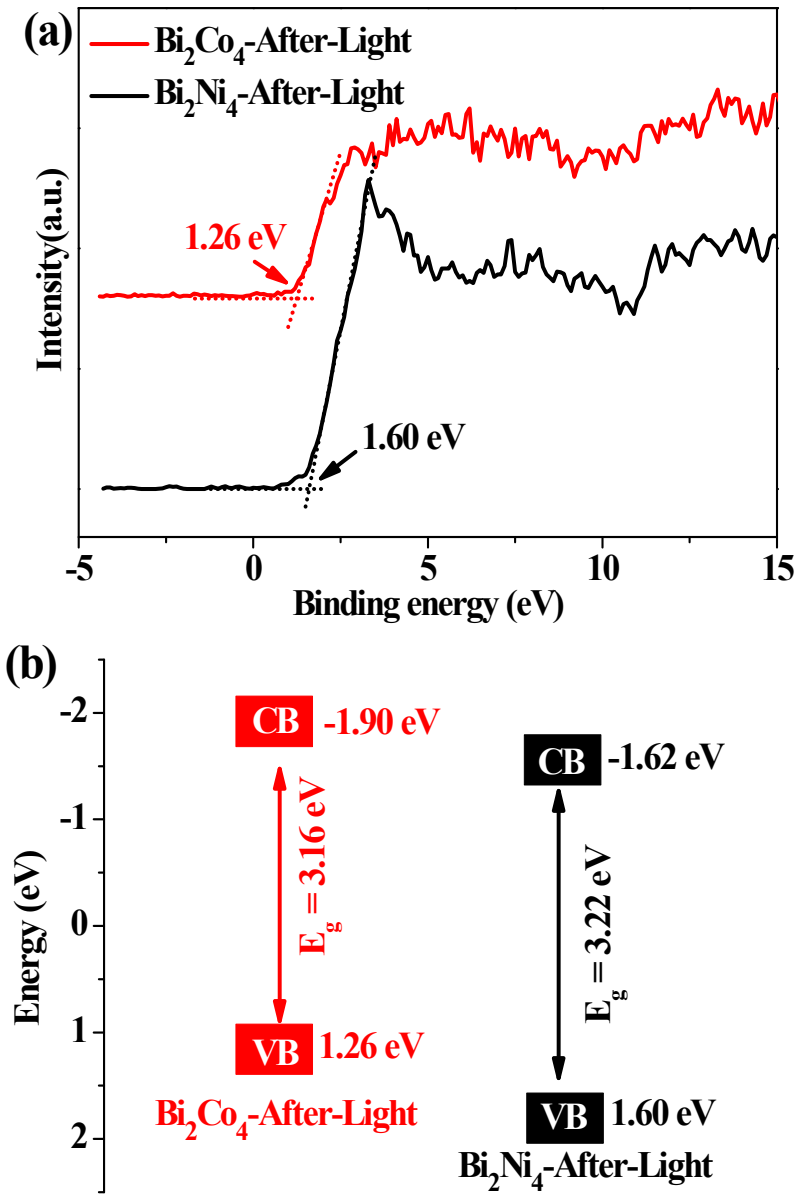

Fig. S7 Bi_2M_4 after photothermal experiment (a) Valence-band spectra; (b) The estimated VB and CB levels.

Calculation of photothermal conversion efficiency

Solid photothermal conversion efficiency determination

a quartz flake (343 mg) was placed over the sample and then the lamp penetrates the quartz to irradiate the sample, the temperature of the quartz flake surface was recorded.

The solid photothermal conversion efficiency (η_s) was calculated according to previous method.[S4,S5] $\eta_{520} = \frac{hs\Delta T_{max}}{I\left(1-10^{-A_{520}}\right)}$, I is the light power density, A_{520} is the absorbance of Bi_2M_4 at 520 wavelength, hs can be calculated based on the formula of $\tau_s = \frac{\sum_i m_i C_{p,i}}{hs}$ where τ_s is sample system time constant, when the light switches off, τ_s can be estimated according to the formula of $\tau_s = \frac{-t}{ln\theta}$, m_i and $C_{p,i}$ are the mass and heat capacity of system component, $\theta = \frac{T-T_{surr}}{T_{max}-T_{surr}}$, where T is the temperature of sample, T_{max} is the maximum system temperature, and T_{surr} is the experiment surrounding temperature.

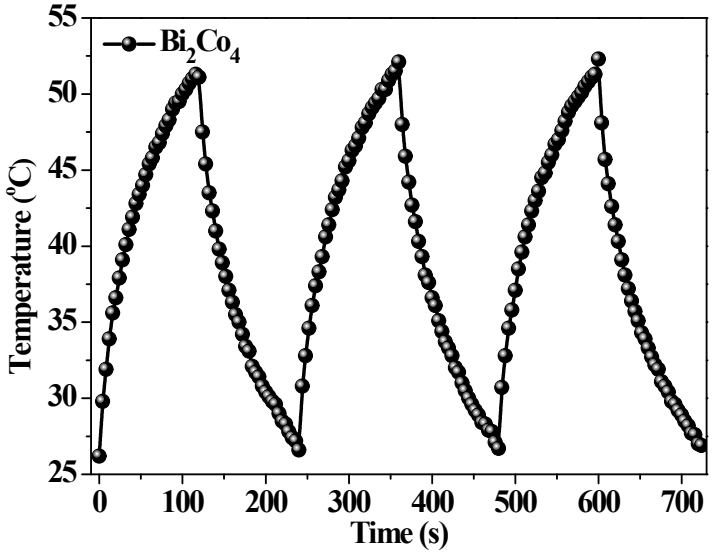

Fig. S8 Time-temperature light on-off cycles of **Bi_2Co_4** for photothermal conversion efficiency determination (520 nm, 0.4 W·cm^{-2})

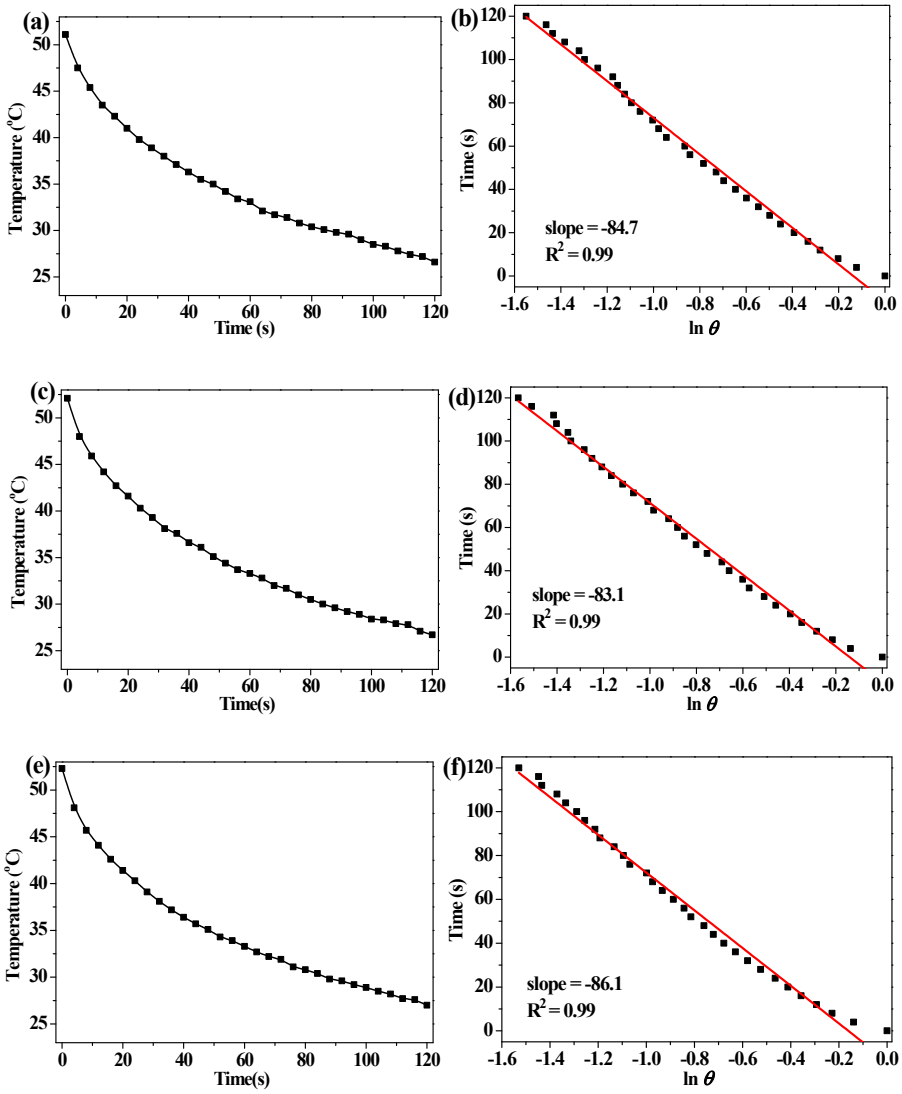

Fig. S9 (a, c, and e) Temperature decay curves of $\mathbf{Bi_2Co_4}$ after removing the light sources of 520 nm (0.4 W·cm^{-2}); (b, d, and f) Linear fit of lnθ-T. Three experiments were conducted in parallel.

The solid photothermal conversion efficiency(η_s) of $\mathbf{Bi_2Co_4}$ was calculated.

For parallel experimental 1 (Figure S9a and S9b): A linear fit of lnθ-T yielded a slope of -84.7, therefore, τ_s was 84.7 s, $\sum_i m_i C_{p,i}$ =0.373 g × 0.8 J (g °C)$^{-1}$ = 0.30 J °C^{-1}, hs = 0.30 / 84.7 = 3.5 × 10^{-3} J·°C^{-1}·s^{-1}, ΔT_{max} = 25.1 °C, A_{520} = 0.203 (Fig. 2a), Eventually, η_1 = 3.5 × 10^{-3} × 25.1 / [0.4 × (1 - 10$^{-0.203}$)] = 59.3 %.

For parallel experimental 2 (Figure S9c and S9d): A linear fit of lnθ-T yielded a slope of -83.1, therefore, τ_s was 83.1 s, $\sum_i m_i C_{p,i}$ =0.0373 g × 0.8 J (g °C)$^{-1}$ = 0.30 J °C^{-1}, hs =

0.30 / 83.1 = 3.6 × 10^{-3} J·^{o}C^{-1}·s^{-1}, ΔT_{max} = 26.1 ^{o}C, A_{520} = 0.203 (Fig. 2a), Eventually, η_2 = 3.6 × 10^{-3} × 26.1 / [0.4 × (1 - $10^{-0.203}$)] = 62.8 %.

For parallel experimental 3 (Figure S9e and S9f): A linear fit of lnθ-T yielded a slope of -86.1, therefore, τ_s was 86.1 s, $\sum_i m_i C_{p,i}$ =0.0373 g × 0.8 J (g ^{o}C)$^{-1}$ = 0.30 J ^{o}C^{-1}, hs = 0.30 / 86.1 = 3.5 × 10^{-3} J·^{o}C^{-1}·s^{-1}, ΔT_{max} = 26.3 ^{o}C, A_{520} = 0.203 (Fig. 2a), Eventually, η_3 = 3.5 × 10^{-3} × 26.3 / [0.4 × (1 - $10^{-0.203}$)] = 61.1 %.

The photothermal conversion efficiency of **Bi_2Co_4** in solid state under 520 nm irradiation is 61.1±1.8 % (The error is based on the standard deviation of three parallel experiments).

The solid photothermal conversion efficiency (η_s) of **Bi_2Ni_4** is 69.4±1.7 % which is calculated by the same method based on the following data (The error is based on the standard deviation of three parallel experiments).

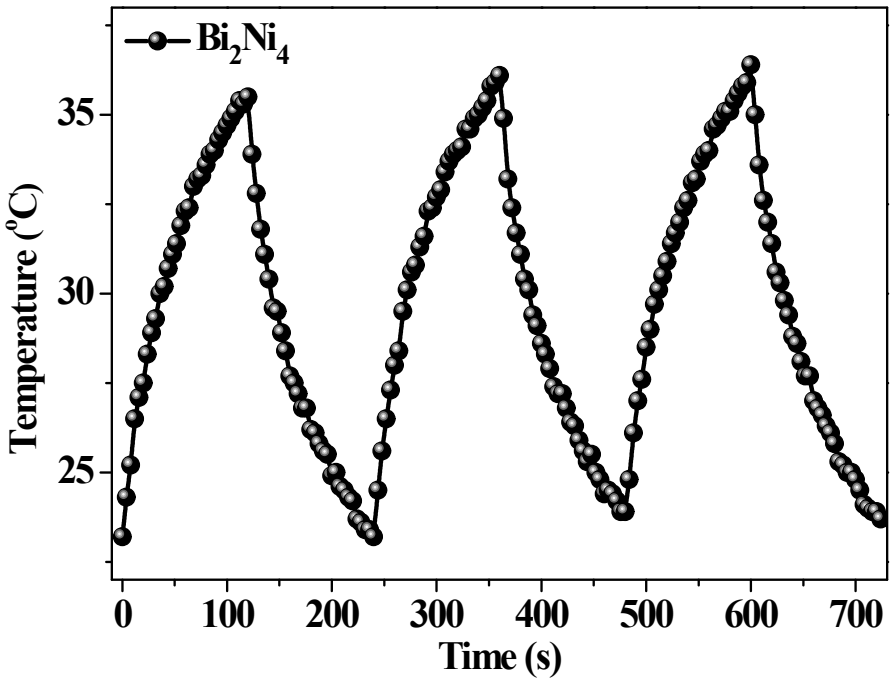

Fig. S10. Time-temperature light on-off cycles of **Bi_2Ni_4** for photothermal conversion efficiency determination. (520 nm, 0.4 W·cm^{-2})

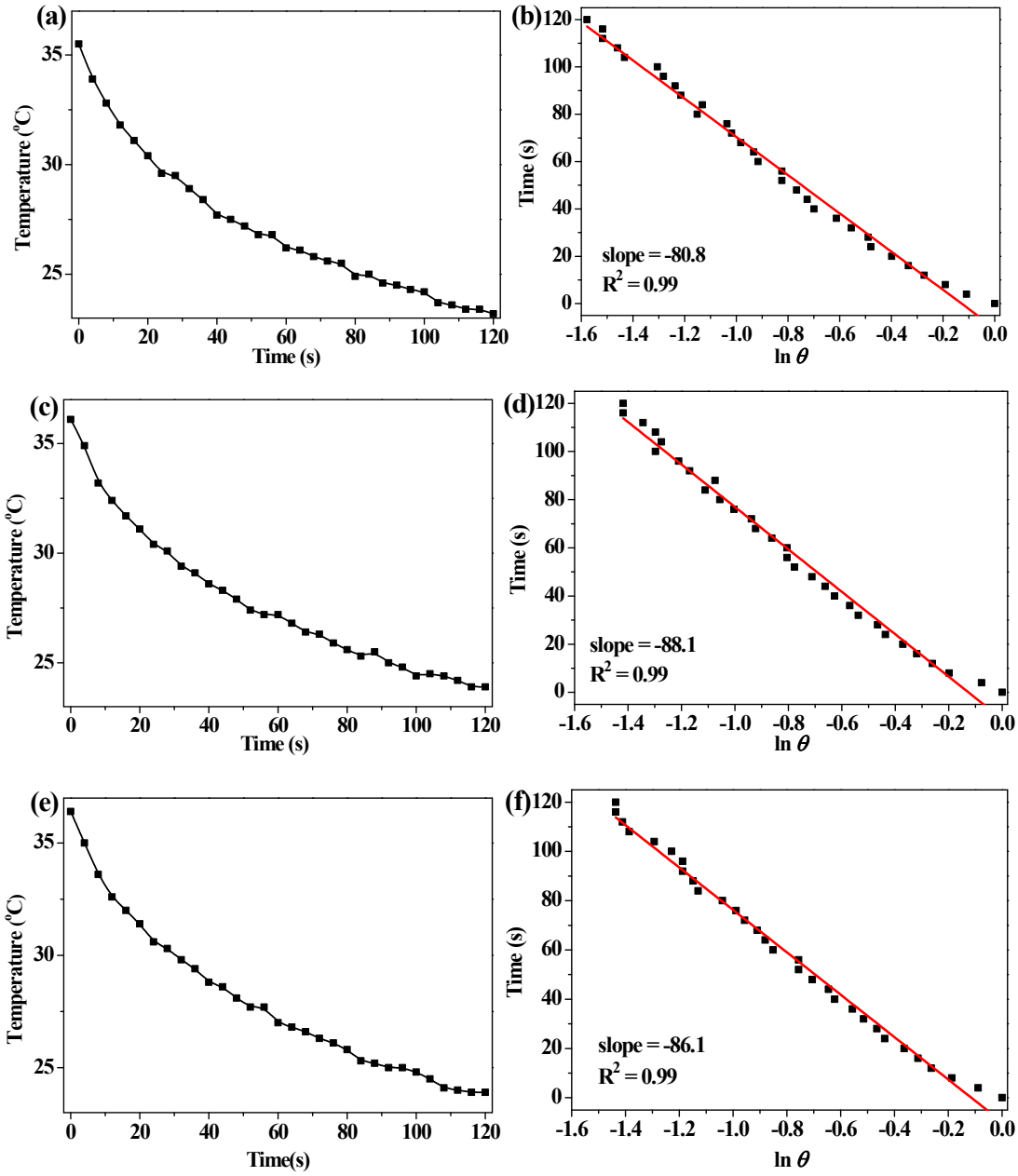

Fig. S11 (a, c, and e) Temperature decay curves of $\mathbf{Bi_2Ni_4}$ after removing the light sources of 520 nm (0.4 W·cm^{-2}); (b, d, and f) Linear fit of lnθ-T. Three experiments were conducted in parallel.

The photothermal conversion efficiency determination in $CHCl_3$

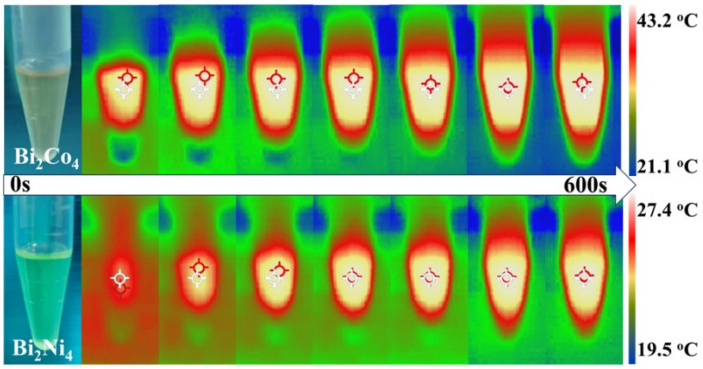

Fig. S12 Photothermal images of Bi_2M_4 in $CHCl_3$ at a concentration of 6 mM. (520 nm, 0.4 W·cm^{-2})

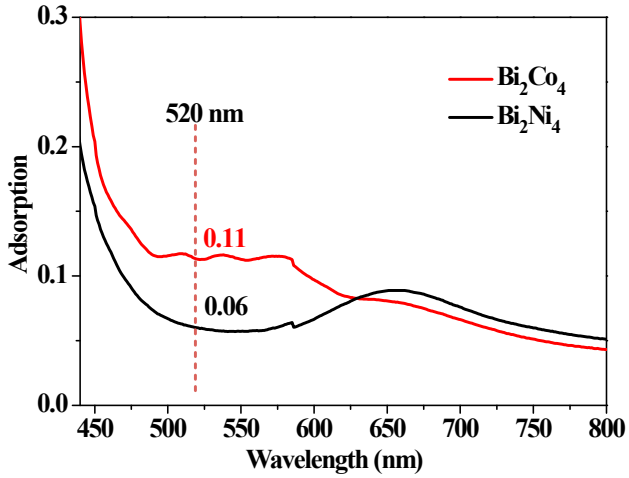

Fig. S13 UV-vis absorption spectra of Bi_2M_4 in $CHCl_3$ at a concentration of 1 mM.

The photothermal conversion efficiency in $CHCl_3$ (η_l) can be calculated by the following equations.[S6-S8]

$$\eta = \frac{hs(\Delta T_{sample} - \Delta T_{solvent})}{I(1 - 10^{-A})}$$

$$hs = \frac{\sum mC_P}{\tau_s}$$

$$\tau_s = \frac{-t}{ln\theta}$$

$$\theta = \frac{(T_{amb} - T)}{(T_{amb} - T_{max})}$$

where h is the heat transfer coefficient, s is the surface area of the container, A is

absorbance of Bi_2M_4 at different wavelength, I is the light power density, m is the mass of sample, C_p is the specific heat capacity of the solvent and t is the time of the cooling process.

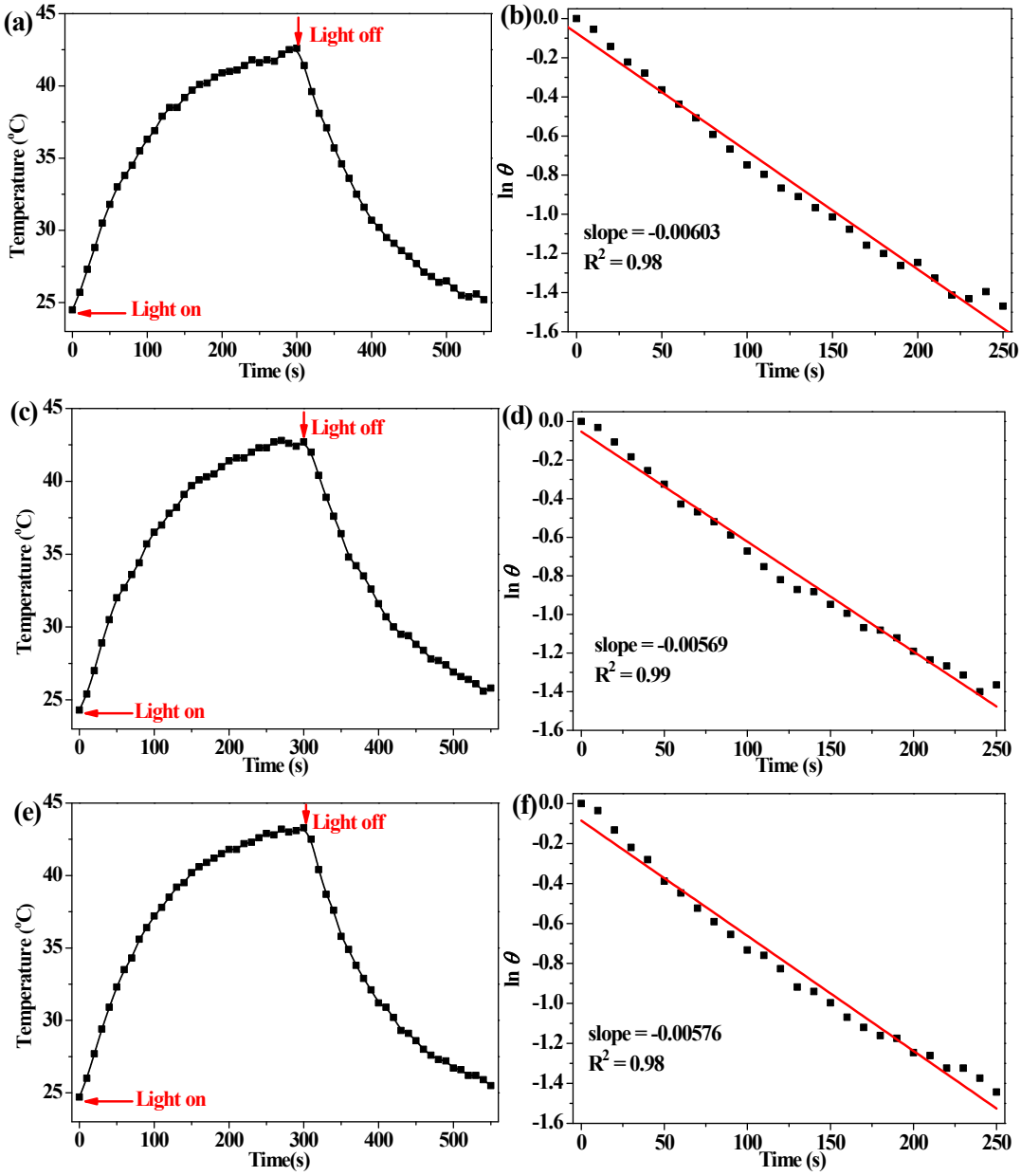

Fig. S14 (a, c, and e) Heating and cooling curve of **Bi_2Co_4** in $CHCl_3$ at a concentration of 6 mM under 520 nm light irradiation (0.4 W·cm^{-2}); (b, d, and f) Linear fit of T-lnθ obtained from cooling curves. Three experiments were conducted in parallel.

The photothermal conversion efficiency (η_l) of **Bi_2Co_4** was calculated.

For parallel experimental 1 (Figure S14a and S14b): A linear fit of T-lnθ yielded a slope of -0.00603, τ_s was calculated as 165.84 s (τ_s = -1/slope). ΣmC_p = $\rho(CHCl_3)\cdot V(CHCl_3)\cdot C_p(CHCl_3)$ = 0.5 mL × 1.48 g/mL × 1.189 J/(g °C^{-1}) = 0.88 J °C^{-1}.

Therefore, hs = 0.88 / 165.84 = 5.31 × 10^{-3} J·°C^{-1}·s^{-1}. ΔT_{sample} = 22.6 °C. $\Delta T_{solvent}$ = 1 °C. A_{520} = 0.11 × 6 = 0.66 (Figure S12). Eventually, η_1 = 5.31 × 10^{-3} × (22.6 - 1) / [0.4 × (1 - $10^{-0.66}$)] = 36.7 %.

For parallel experimental 2 (Figure S14c and S14d): A linear fit of T-lnθ yielded a slope of -0.00569, τ_s was calculated as 175.75 s (τ_s = -1/slope). ΣmC_p = $\rho(CHCl_3)\cdot V(CHCl_3)\cdot C_p(CHCl_3)$ = 0.5 mL × 1.48 g/mL × 1.189 J/(g °C^{-1}) = 0.88 J °C^{-1}. Therefore, hs = 0.88 / 175.75 = 5.01 × 10^{-3} J·°C^{-1}·s^{-1}. ΔT_{sample} = 22.7 °C. $\Delta T_{solvent}$ = 1 °C. A_{520} = 0.11 × 6 = 0.66 (Figure S12). Eventually, η_2 = 5.01 × 10^{-3} × (22.7 - 1) / [0.4 × (1 - $10^{-0.66}$)] = 34.8 %.

For parallel experimental 3 (Figure S14e and S14f): A linear fit of T-lnθ yielded a slope of -0.00576, τ_s was calculated as 173.61 s (τ_s = -1/slope). ΣmC_p = $\rho(CHCl_3)\cdot V(CHCl_3)\cdot C_p(CHCl_3)$ = 0.5 mL × 1.48 g/mL × 1.189 J/(g °C^{-1}) = 0.88 J °C^{-1}. Therefore, hs = 0.88 / 173.61 = 5.07 × 10^{-3} J·°C^{-1}·s^{-1}. ΔT_{sample} = 23.2 °C. $\Delta T_{solvent}$ = 1 °C. A_{520} = 0.11 × 6 = 0.66 (Figure S12). Eventually, η_3 = 5.07 × 10^{-3} × (23.2 - 1) / [0.4 × (1 - $10^{-0.66}$)] = 36.2 %.

The η_l of **Bi_2Co_4** at a concentration of 6 mM is 35.9±1.0 % (The error is based on the standard deviation of three parallel experiments).

The photothermal conversion efficiency (η_l) of **Bi_2Ni_4** at a concentration of 6 mM was calculated using the same method based following data. The η_l value is 7.7±0.2 % (The error is based on the standard deviation of three parallel experiments).

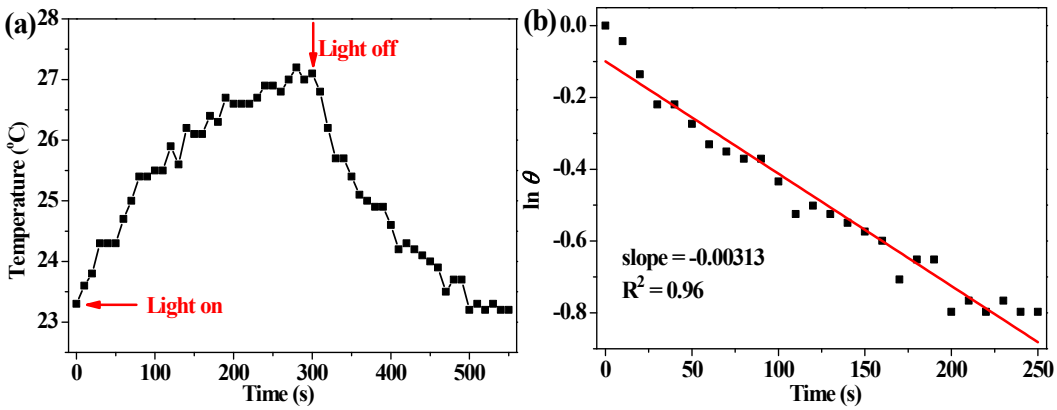

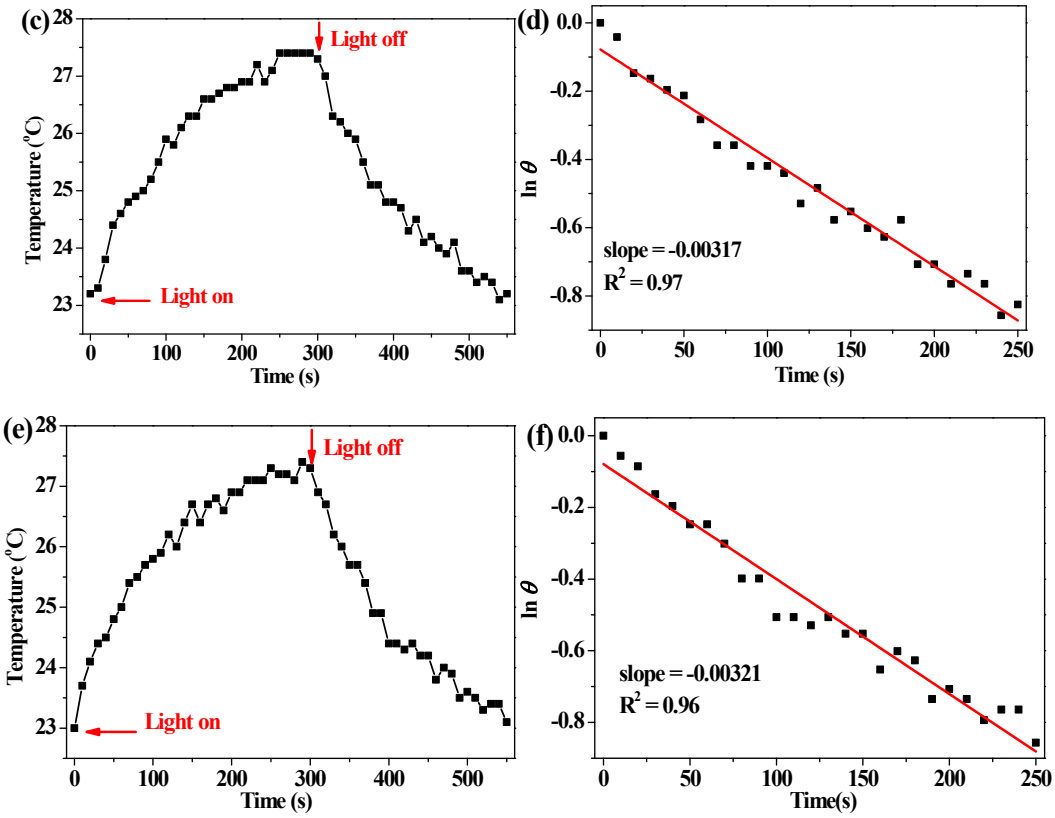

Fig. S15 (a, c, and e) Heating and cooling curve of **Bi_2Ni_4** in $CHCl_3$ at a concentration of 6 mM under 520 nm light irradiation (0.4 W·cm^{-2}); (b, d, and f) Linear fit of *T*-lnθ obtained from cooling curves. Three experiments were conducted in parallel.

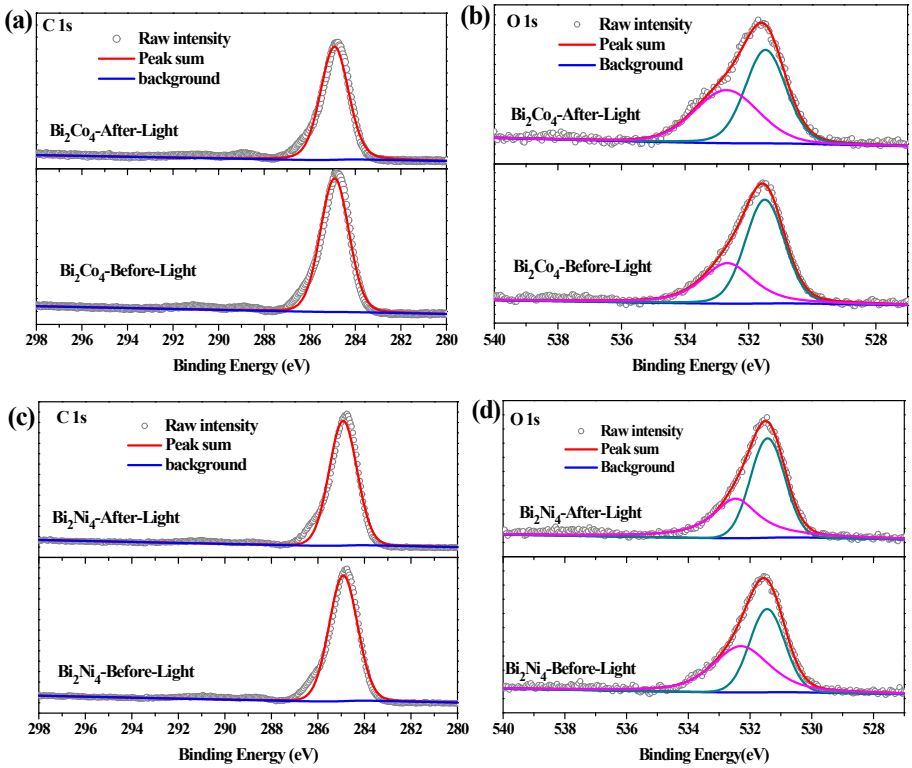

Fig. S16 High-resolution spectra of (a and c) C1s of Bi_2M_4 ;(b and d) O 1s of Bi_2M_4.

Table S1. Crystal data for Bi_2M_4 (M = Co or Ni).

Complex	**Bi_2Co_4**	**Bi_2Ni_4**
Formula	$C_{164}H_{186}Bi_2Co_4O_{20}S_{16}$	$C_{164}H_{186}Bi_2Ni_4O_{20}S_{16}$
Formula weight [c]	3643.94	3642.88
Crystal system	triclinic	triclinic
Space group	*P*$\bar{1}$ (No. 2)	*P*$\bar{1}$ (No. 2)
a(Å)	13.814(4)	13.8454(10)
b(Å)	18.929(5)	19.0729(13)
c(Å)	19.532(5)	19.6074(14)
α(°)	67.633(10)	67.170(3)
β(°)	81.377(11)	80.576(3)
γ(°)	86.179(10)	85.808(3)
Volume(Å^3)	4669(2)	4707.5(6)
Z	1	1
Temperature (K)	296	296
Dc(g/cm^3)[c]	1.296	1.285
μ(mm^{-1})[c]	2.46	2.49
Reflections collected	45659	44353
Unique data	17210	16622
R_{int}	0.035	0.060
GOF on F^2	1.031	1.035
[a]R_1[I>2sigma(I)]	0.0369	0.0577
[b]wR_2	0.1065	0.1682

[a]$R_1 = \Sigma||F_0|-|F_c||/\Sigma|F_0|$; [b]$wR_2 = \{\Sigma[w(F_0^2-F_c^2)^2]/\Sigma[w(F_0^2)^2]\}^{1/2}$. [c]The solvent molecules are not included.

Table S2. Selected bond length (Å) and bond valance calculations (BVS) for Bi_2M_4 (M = Co or Ni)

Bond	M = Co			M = Ni		
	Distance	r	value	Distance	r	value
Bi1-O7	2.271(3)	2.09	0.613	2.284(4)	2.09	0.592
Bi1-O9	2.320(3)	2.09	0.537	2.316(5)	2.09	0.543
Bi1-O2	2.350(3)	2.09	0.495	2.382(4)	2.09	0.454
Bi1-O8	2.567(3)	2.09	0.275	2.549(4)	2.09	0.289
Bi1-O10	2.615(3)	2.09	0.242	2.601(5)	2.09	0.251
Bi1-O3	2.713(3)	2.09	0.186	2.699(5)	2.09	0.193
Bi1-S8	2.8075(12)	2.55	0.499	2.8078(17)	2.55	0.498
Valence			2.847	Valence		2.821
Bond	Distance	r	value	Distance	r	value
M1-O4	2.006(3)	1.692	0.428	2.030(5)	1.654	0.362
M1-O8	2.083(3)	1.692	0.348	2.048(4)	1.654	0.345
M1-O5	2.115(3)	1.692	0.319	2.059(5)	1.654	0.335
M1-O1	2.046(3)	1.692	0.384	2.064(4)	1.654	0.330
M1-S1	2.4576(13)	2.06	0.341	2.382(2)	2.04	0.397
M1-S5	2.5048(13)	2.06	0.301	2.446(2)	2.04	0.334
Valence			2.120	Valence		2.102
Bond	Distance	r	value	Distance	r	value
M2-O6	2.013(3)	1.692	0.420	2.013(5)	1.654	0.379
M2-O7	2.000(3)	1.692	0.435	2.015(4)	1.654	0.377
M2-O2	2.092(3)	1.692	0.339	2.023(4)	1.654	0.369
M2-O1	2.115(3)	1.692	0.319	2.127(4)	1.654	0.278
M2-S2	2.4302(13)	2.06	0.368	2.3635(19)	2.04	0.417
M2-S7	2.6489(14)	2.06	0.204	2.608(2)	2.04	0.215
Valence			2.06	Valence		2.04
Symmetry code:(a) -x,1-y,1-z;(b) -x, -y,1-z; (c)1-x,1-y,1-z						

Table S3. The Selected bond angles for Bi_2M_4 (M = Co or Ni)

Bond angle	M = Co	M = Ni
M1—O1—M2	121.11 (13)	123.0 (2)
M2—O2—Bi1	102.59 (11)	102.64 (18)
M2—O7—Bi1	108.54 (12)	106.40 (19)
M1—O8—Bi1	120.48 (12)	120.65 (19)
Bi1—O10—Bi1	117.30(125)	118.15(219)

References

S1 B. S. Hou, H. Y. Zheng, K. H. Zhang, Q. Wu, C. Qin, C. Y. Sun, Q. H. Pan, Z. H.Kang, X. L. Wang and Z. M. Su, Electron delocalization of robust high-nuclear bismuth-oxo clusters for promoted CO_2 electroreduction, *Chem. Sci.*, 2023, **14,** 8962-8969.

S2 H.-N. Zhou, Q.-Y. Liu, X.-Y. Chen, J.-G. Xu, L.-Y. Li, K.-Y. Liu, J. Yan and C. Liu, In Situ Oxidative Ring-Opening of Calix[8]arene to Construct Stable Bismuth-Oxo Clusters with Exposed Catalytic Sites for Specific Electroreduction of CO_2 to HCOOH, *Inorg. Chem.*, 2024, **63,** 20501-20509.

S3 M. Liu and W. Liao, Bridging calixarene-based $\{Co_4\}$ units into a square or belt with aromatic dicarboxylic acids, *CrystEngComm*, 2012, **14,** 5727-5729.

S4 S. Wang, S. Li, J. Xiong, Z. Lin, W. Wei and Y. Xu, Near-infrared photothermal conversion of stable radicals photoinduced from a viologen-based coordination polymer, *Chem. Commun.*, 2020, **56,** 7399-7402.

S5 N.-N. Zhang, Y.-T. Liu, L. Li, X.-T. Liu, K. Xu, Z.-Y. Li and Y. Yan, Highly efficient NIR-II photothermal conversion from a 2,2′-biquinoline-4,4′-dicarboxylate-based photochromic complex, *Inorg. Chem. Front.*, 2024, **11,** 4867-4875.

S6 G. Yang, X. Mu, X. Pan, Y. Tang, Q. Yao, Y. Wang, F. Jiang, F. Du, J. Xie, X. Zhou and X. Yuan, Ligand engineering of Au_{44} nanoclusters for NIR-II luminescent and photoacoustic imaging-guided cancer photothermal therapy, *Chem. Sci.*, 2023, **14,** 4308-4318.

S7 Z. Wang, Y. Wang, C. Zhang, Y.-J. Zhu, K.-P. Song, C. M. Aikens, C.-H. Tung and D. Sun, Silvery fullerene in Ag_{102} nanosaucer, *Natl. Sci. Rev.*, 2024, **11**, nwae192.

S8 L. Fang, W. Fan, G. Bian, R. Wang, Q. You, W. Gu, N. Xia, L. Liao, J. Li, H. Deng, N. Yan and Z. Wu, Sandwich-Kernelled AgCu Nanoclusters with Golden Ratio Geometry and Promising Photothermal Efficiency, *Angew. Chem. Int. Ed.*, 2023, **62,** e202305604.